Research Article

Received: 26 June 2012 Revised: 10 October 2012 Accepted: 11 October 2012 Published online in Wiley Online Library:

(wileyonlinelibrary.com) DOI 10.1002/jctb.3984

Evaluation of Ba-promoted Mo carbide catalyst for Fischer–Tropsch synthesis

Dai-Viet N. Vo,[a,c] Viswanathan Arcotumapathy,[a] Bawadi Abdullah[b] and Adesoji A. Adesina[a*]

Abstract

BACKGROUND Traditional FT catalysts such as Co and Fe still suffer from carbon-induced deactivation even with alkali promotion. The objective of this study was to examine the effect of Ba addition to carbon-tolerant Mo carbide since it has Pt-like characteristics and is cheaper than noble metals as an FT catalyst.

RESULTS The presence of Ba increased the Mo carbide production rate and reduced the activation energy for its formation. The promoted catalyst exhibited higher specific basic site strength and CO_2 uptake for strong basic site than that of the undoped catalyst. Both catalysts exhibited optimal reaction rate at a H_2 mole fraction of 0.75 while CO consumption rate, total olefin-to-paraffin ratio, methane suppression as well as C_{5+} selectivity were improved with Ba addition. The non-standard Anderson–Schulz–Flory (ASF) product distribution observed for the Ba-doped catalyst may be due to the appearance of an additional polymerization site on the catalyst surface located in the $BaMoO_4$ phase. Chain growth factor was enhanced by up to 93% from 0.43 to 0.83 with the Ba-doped catalyst.

CONCLUSIONS Ba promoter increased chain growth probability by about 93%. The deviation of product distribution from standard ASF plots with 2 chain growth factors for the 3wt%Ba-10%MoC_{1-x}/Al_2O_3 catalyst was probably due to the presence of different active sites for chain initiation. The result is unprecedented and represents excellent opportunity for industrial exploitation of a new and relatively cheap carbon-resistant catalyst.

Keywords: Fischer–Tropsch synthesis; molybdenum carbide; temperature-programmed carburization; Ba-promotion

INTRODUCTION

Fischer–Tropsch synthesis (FTS) is now regarded as a viable alternative for clean energy production and a substitute for petroleum-based energy due to increasing crude oil price and the availability of cheap, large reserves of natural gas. While conventional FT (Co- and Fe-based) catalysts are generally intolerant of carbon deposition and sulphur-containing compounds in feed gas,[1] molybdenum carbide catalyst has been receiving significant attention due to its high carbon resistance, sulphur resilience[2,3] and olefin selectivity[4] since it has been found to possess similar catalytic properties to noble metals.[5] In fact, MoC_{1-x} ($0 \leq x < 1$) catalyst has been employed for different catalytic reactions including NH_3 synthesis,[6] NO reduction,[7] reforming,[8,9] water-gas-shift reaction,[10] hydrotreating[11,12] and particularly CO hydrogenation.[13–15]

Several methods, including metal precursor pyrolysis,[16] sonochemical synthesis,[17] alkalide reduction[18] and solution-derived precursor[19] have been used for Mo carbide catalyst synthesis. However, temperature-programmed carburization developed by Boudart and co-workers[20,21] seems to be the most common method to produce MoC_{1-x} with high surface area. Conventionally, a mixture of H_2/CH_4 is employed as carbon source to produce Mo carbide catalyst from MoO_3 precursor at a temperature greater than 1073 K.[3] However, the utilization of higher alkanes, C_{2+} reportedly facilitated carburization at lower reaction temperatures and hence improved solid BET surface area.[22,23] Xiao *et al*. found that carburization conditions and carburizing agents influenced the physicochemical attributes, structure and catalytic performance of Mo carbide catalysts.[22] H_2/C_3H_8 mixture has been used for MoC_{1-x}/Al_2O_3 catalyst synthesis with high surface area of 92–204 $m^2\ g_{cat}^{-1}$ from a metal sulphide precursor.[24] Vo *et al*. reported that H_2/C_3H_8=5:1 was the optimal carburizing feed for the highest carbide formation rate and FT activity.[25,26] Therefore, in this study, a $5H_2/1C_3H_8$ mixture was utilized for Mo carbide catalyst production. Conventionally, FT catalysts are promoted with basic metal (alkali) oxides for chain growth probability and CO consumption rate enhancement.[27] Hence, Mo carbide catalyst would also benefit from similar promoters. In previous studies, Vo *et al*. found that K-promoted MoC_{1-x}/Al_2O_3 catalyst exhibited higher FT activity and

* *Correspondence to: A.A. Adesina, Reactor Engineering & Technology Group, School of Chemical Engineering, The University of New South Wales, Sydney, Australia 2052. E-mail: a.adesina@unsw.edu.au*

a *Reactor Engineering & Technology Group, School of Chemical Engineering, The University of New South Wales, Sydney, Australia 2052,*

b *Chemical Engineering Department, Universiti Teknologi PETRONAS, 31750, Tronoh, Perak, Malaysia*

c *Chemical Engineering Program, Texas A&M University at Qatar, P.O. Box 23874, Doha, Qatar*

chain growth factor than those of unpromoted catalyst probably due to increased basic site concentration.[28] Although alkaline-earth promoters also possess basic properties, these metals have not been employed as dopants for Mo carbide catalyst before. Therefore, the aim of this research was to investigate the effect of Ba promoter on both physicochemical properties and FT performance of Mo carbide catalyst prepared by temperature-programmed carburization with the optimal ($5H_2/1C_3H_8$) carburizing feed.

EXPERIMENTAL

The 10wt%MoO_3/Al_2O_3 and 3wt%Ba-10wt%MoO_3/Al_2O_3 catalysts were prepared by impregnation method with $(NH_4)_6Mo_7O_{24}.4H_2O$ and $Ba(NO_3)_2$ as precursor solutions. γ-Al_2O_3 support (provided by Saint-Gobain NorPro) thermally pretreated at 973 K in air for 6 h to ensure thermal stability was mixed with a calculated amount of aqueous $(NH_4)_6Mo_7O_{24}.4H_2O$ solution for 3 h. The impregnated solution was subsequently dried in an oven for 16 h at 403 K (referred to as uncalcined solid sample, UC-CAT) and calcined in air at 773 K for 5 h to produce 10%MoO_3/Al_2O_3 catalyst. This catalyst was further mixed with $Ba(NO_3)_2$ promoter solution followed by similar drying and calcination steps to synthesize a 3%Ba–10%MoO_3/Al_2O_3 catalyst. About 0.15 g of Ba-promoted or unpromoted Mo oxide catalyst was carburized with 50 ml min^{-1} of $5H_2/1C_3H_8$ at 973 K and 10 K min^{-1} for 2 h in a computer-controlled fixed bed reactor for corresponding Ba-promoted or unpromoted 10%MoC_{1-x}/Al_2O_3 catalyst formation. The catalyst bed was subsequently cooled down to FT reaction temperature in N_2 flow at the end of carburization runs. Fischer–Tropsch synthesis evaluation was carried out *in situ* in the same reactor with different H_2/CO ratios of 5:1 to 1:5 at 473 K and atmospheric pressure. The ends of reactor were covered with fibre glass insulation to minimize heat loss and to prevent product condensation. The reactor exit line was also heated up to 473 K using heating tapes to ensure that long chain hydrocarbon products were kept in gas phase for online gas chromatograph (Shimadzu GC-17A equipped with FID detector and Alltech AT-1 capillary column) measurement. CO conversion, X_{CO} was estimated as;

$$X_{CO} = \frac{\begin{array}{c}\textit{Total carbon in the production rates}\\ \textit{for all hydrocarbon products measured}\end{array}}{\textit{Total rate of CO fed}} \times 100\% \quad (1)$$

A mean catalyst particle size of 100 μm and gas hourly space velocity (GHSV) of 10 L g_{cat}^{-1} h^{-1} were employed for all reactions to ensure negligible internal and external transport resistances.

The Quantachrome Autosorb-1 unit was used to measure catalyst surface area, pore volume and pore diameter by nitrogen physisorption at 77 K. X-ray diffraction of Mo carbide catalysts was performed in a Philips X'pert Pro MPD system using Ni-filtered Cu Kα (λ= 1.542 Å) at 45 kV and 40 mA. Thermogravimetric analysis runs including temperature-programmed calcination and carburization were carried out in a ThermoCahn TGA 2121 unit. In temperature-programmed calcination, about 70 mg of the UC-CAT solid sample placed in a quartz sample boat was pretreated in argon flow for volatile compounds and moisture removal by heating to 393 K and maintaining at this temperature for 30 min. MoO_3/Al_2O_3 precursors were subsequently calcined in high purity air (50 mL min^{-1}) from 393–973 K at 10 K min^{-1} and kept isothermally at 973 K for 1 h before cooling down to 303 K in inert gas. Temperature-programmed carburization runs were performed between promoted or unpromoted MoO_3/Al_2O_3 catalyst and a mixture of $5H_2/1C_3H_8$ from 303 to 973 K with different heating rates (10–20 K min^{-1}). NH_3- and CO_2-temperature-programmed desorption (NH_3- and CO_2-TPD) measurements for heat of desorption and site concentration estimation of acid and basic centers, respectively, were conducted on a Micromeritics 2910 AutoChem unit with ramping rates of 5–30 K min^{-1}. Approximately 0.15 g of catalyst sample sandwiched between layers of quartz wool in a U-tube was exposed to a flow of 10%NH_3 or 10%CO_2 diluted in inert gas for 1 h followed by controlled heating to 973 K with different heating rates of 5–30 K min^{-1}.

RESULTS AND DISCUSSION

X-ray diffraction and BET measurements

The X-ray diffractograms of Ba-promoted and undoped 10%MoC_{1-x}/Al_2O_3 catalysts are shown in Fig. 1. XRD patterns were analyzed based on the Joint Committee on Powder Diffraction Standards (JCPDS) database.[29] The high intensity peaks detected at 2θ= 45.7° and 66.8° were assigned to the γ-Al_2O_3 support. Both promoted and unpromoted catalysts possessed face-centered cubic (FCC) α-MoC_{1-x} (2θ= 36.6° and 61.3° for [111] and [220], respectively) and hexagonal closed packed (HCP) β-MoC_{1-x} (2θ= 34.0° and 39.5°) phases. As seen in Fig. 1(b), the peak located at 2θ=26.5° may belong to deposited carbon while the $BaMoO_4$ phase (with typical peak at 2θ= 32.1°) was formed on catalyst surface indicating the interaction between BaO promoter and MoO_3 precursor may be given as

$$Ba(NO_3)_2 \rightarrow BaO + 2NO_2 + \frac{1}{2}O_2 \quad (2)$$

$$BaO + MoO_3 \rightarrow BaMoO_4 \quad (3)$$

There were no detectable peaks for the MoO_3 phase (with 2θ= 23.40°, 25.50° and 26.75°) on Mo carbide catalysts suggesting the complete conversion of Mo oxide to MoC_{1-x} phases during carburization. This observation is supported by previous studies,[30] while the absence of metal (Ba or Mo) aluminates at the calcination temperature is also consistent with findings of Szalier *et al.*[31]

The average MoC_{1-x} crystallite size, d_p (cf. Table 1) may be estimated from the XRD pattern via the Scherrer equation:[32]

$$d_p = \frac{0.9\lambda}{B\cos\theta} \quad (4)$$

where λ and B are wavelength and peak width, respectively, while θ is the Bragg angle. The d_p reduced with Ba promotion from 9.8 to 6.1 nm. The small average MoC_{1-x} particle size of less than 10 nm suggested that MoC_{1-x} particles were well dispersed on the support surface. In fact, the BET surface area of Mo carbide catalysts is close to that of Al_2O_3 support, further supporting the conclusion of fine MoC_{1-x} dispersion. Promoted and unpromoted Mo carbide catalysts possessed greater surface area than that of corresponding MoO_3 precursors. The addition of Ba promoter reduced BET surface area of both MoO_3 precursor (from 182.4 to 156.9 m^2 g_{cat}^{-1}) and MoC_{1-x} catalyst (from 194.0 to 169.8 m^2 g_{cat}^{-1}), most likely due to pore blockage.

Table 1. Summary of physical properties of the Mo carbide catalyst system

Catalyst	Average BET surface area ($m^2\ g_{cat}^{-1}$)	Average pore volume ($cm^3\ g_{cat}^{-1}$)	Average pore diameter (nm)	Average crystallite size*(nm)
Calcined pure Al_2O_3	179.3±0.9	0.68±0.01	15.2±0.2	-
10%MoO_3/Al_2O_3	182.4±1.8	0.55±0.01	12.0±0.1	-
10%MoC_{1-x}/Al_2O_3	194.0±1.9	0.73±0.01	15.0±0.2	9.80
3%Ba-10%MoO_3/Al_2O_3	156.9±0.8	0.66±0.01	16.8±0.2	-
3%Ba–10%MoC_{1-x}/Al_2O_3	169.8±1.7	0.71±0.01	16.6±0.2	6.11

*Average crystallite size was estimated from XRD patterns using the Scherrer equation.

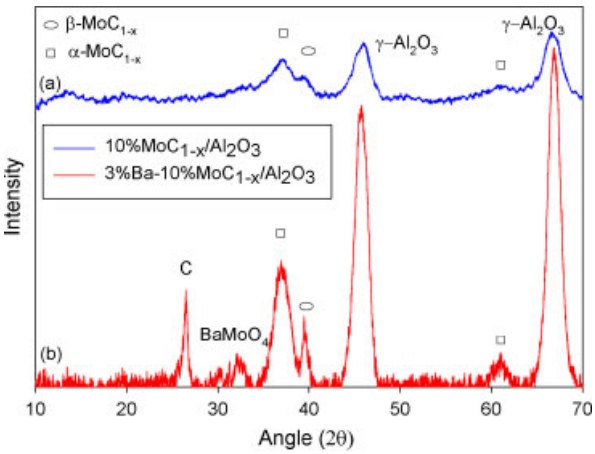

Figure 1. XRD patterns of (a) unpromoted and (b) Ba-promoted Mo carbide catalysts.

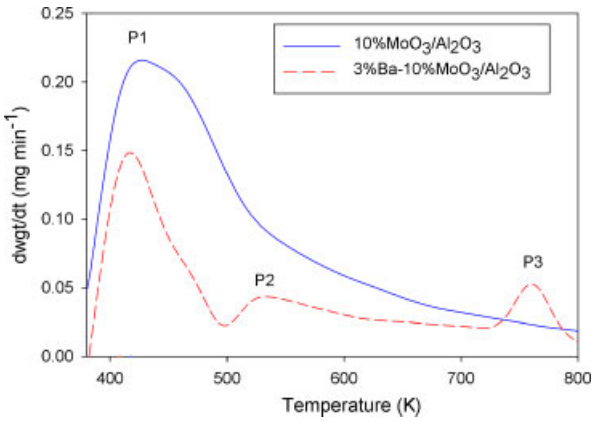

Figure 2. Derivative weight profiles for temperature-programmed calcination of promoted and unpromoted 10%MoO_3/Al_2O_3 catalysts at 10 K min^{-1}.

Thermogravimetric studies

Derivative weight profiles for temperature-programmed calcination runs of alumina-supported MoO_3 precursors are illustrated in Fig. 2. The low temperature peak (P1) at 418–427 K was probably due to the formation of MoO_3 precursor from $(NH_4)_6Mo_7O_{24}$ thermal decomposition:

$$(NH_4)_6\,Mo_7O_{24} \rightarrow 6NH_3 + 7MoO_3 + 3H_2O \qquad (5)$$

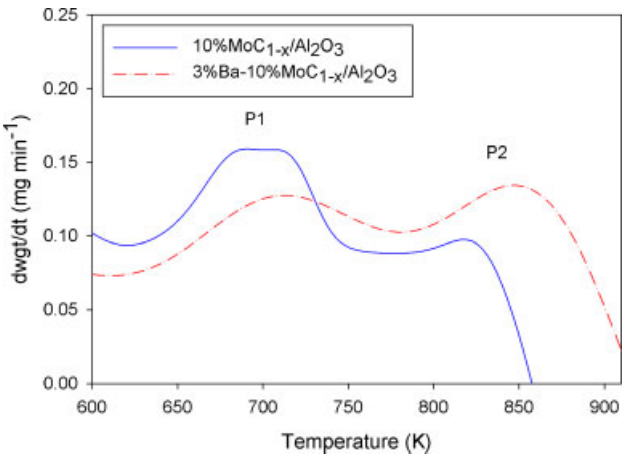

Figure 3. Derivative weight profiles for temperature-programmed carburization of promoted and unpromoted 10%MoC_{1-x}/Al_2O_3 catalysts at 20 K min^{-1}.

while peaks P2 (531 K) and P3 (760 K) in promoted MoO_3/Al_2O_3 catalyst were ascribed to *BaO* and *$BaMoO_4$* formation, respectively (cf. Equations (2) and (3)).

Figure 3 shows the effect of Ba promoter on temperature-programmed carburization runs between promoted and unpromoted 10%MoO_3/Al_2O_3 with $5H_2/1C_3H_8$. It was evident that the carburization was a two-step process with the formation of an intermediate oxycarbide form (low temperature peak, P1 at 730–713 K) and the final carbide phase (P2 at 820–848 K). This observation is in agreement with other studies.[24,33,34] The Arrhenius parameters for oxycarbide and carbide phase formation estimated from the Kissinger equation[35] (cf. Equation (6)) are summarized in Table 2.

$$\ln\left(\frac{\beta}{T_P^2}\right) = \ln\left(\frac{AR}{E_a}\right) - \frac{E_a}{RT_P} \qquad (6)$$

with β, T_P and R being heating rate, peak temperature and universal gas constant, respectively.

The activation energy E_a for carbide phase formation was higher than that of oxycarbide formation for doped and undoped catalysts suggesting that oxycarbide formation from MoO_3 during carburization was more facile than the final carbide phase. Although the carburization profile shifted to high temperature with promoter addition, Ba-promoted catalyst exhibited a higher carbide formation rate (cf. Fig. 3) due to a reduction in the E_a values of both carbide phases for Ba-doped catalyst as seen in Table 2.

Table 2. Estimates of activation energy E_a and pre-exponential factor A derived from temperature-programmed carburization runs at different heating rates of 10–20 K min^{-1} for the formation of oxycarbide and carbide phases

	Oxycarbide (Peak P1)		Carbide phase (Peak P2)	
Catalyst	Activation energy, E_a (kJ mol^{-1})	Pre-exponential factor, A (s^{-1})	Activation energy, E_a (kJ mol^{-1})	Pre-exponential factor, A (s^{-1})
$10\%MoC_{1-x}/Al_2O_3$	92.39±2.34	$4.75\pm0.12\times10^6$	176.56±3.57	$1.09\pm0.02\times10^{11}$
$3\%Ba-10\%MoC_{1-x}/Al_2O_3$	65.44±0.99	$4.12\pm0.06\times10^4$	111.14±1.12	$6.22\pm0.06\times10^6$

Table 3. Physicochemical attributes of both promoted and unpromoted $10\%MoC_{1-x}/Al_2O_3$ catalysts

Catalyst		$10\%MoC_{1-x}/Al_2O_3$	$3\%Ba-10\%MoC_{1-x}/Al_2O_3$	Al_2O_3 support
NH_3 uptake, A_{NH_3} (mol NH_3 $m^{-2}\times10^7$)	W	6.65	4.22	10.50
	S	11.40	6.42	-
Heat of desorption for NH_3, $E_{d_{NH_3}}$ (kJ mol^{-1})	W	37.91	47.94	50.00
	S	320.12	70.82	-
Specific acid site strength (kJ $m^{-2}\times10^5$)	W	2.52	2.02	5.24
	S	36.60	4.55	-
CO_2 uptake, A_{CO_2} (mol CO_2 $m^{-2}\times10^7$)	W	1.40	0.44	1.47
	S	0.32	2.99	0.91
Heat of desorption for CO_2, $E_{d_{CO_2}}$ (kJ mol^{-1})	W	34.91	25.80	50.00
	S	137.07	83.66	57.42
Specific basic site strength (kJ $m^{-2}\times10^5$)	W	0.49	0.11	0.74
	S	0.44	2.50	0.52
Acid: basic site ratio	W	4.74	9.69	7.12
	S	35.81	2.15	-

Physicochemical properties

The physicochemical properties of Mo carbide catalysts are summarized in Table 3. NH_3- and CO_2-TPD measurements showed that weak (W) and strong (S) acid as well as basic sites were detected on both promoted and unpromoted Mo carbide catalysts. NH_3 desorption was observed at 520–580 K and 690–730 K for weak and strong acid sites, respectively, while peaks for CO_2 desorption were found at about 446–506 K (for weak basic center) and 664–720 K (for strong basic center). The calcined pure Al_2O_3 support also possessed a weak acid site suggesting the strong acid site may belong to MoC_{1-x} phase formation or the interaction between MoC_{1-x} and the Al_2O_3 support. As seen in Table 3, heat of desorption, E_d for strong acid and basic sites was higher than that of weak sites. CO_2 uptake and specific basic site strength of strong basic site were improved with dopant addition probably due to increasing electron density (donated by Ba promoter) on catalyst surface facilitating CO_2 adsorption,[36,37] while a reduction in NH_3 uptake, heat of desorption and specific site strength of the S-acid site was also observed for the promoted catalyst. The ratio of acid-to-basic site concentration seemed to be higher than unity for weak and strong sites of both promoted and unpromoted Mo carbide catalysts indicating that MoC_{1-x} surface is primarily acidic.

Fischer–Tropsch synthesis evaluation

Influence of feed composition

The effect of feed composition on CO consumption rate ($-r_{CO}$) and total olefin-to-paraffin ratio (*TOPR*) of the Mo carbide catalysts is shown in Fig. 4. Both catalysts exhibited similar ($-r_{CO}$)-feed composition profiles with optimal reaction rate at H_2 mole fraction y_{H_2} of 0.75. CO consumption rate improved with Ba promoter about 2 times for all feed compositions probably due to increasing strong basic site concentration (CO_2 uptake) as seen in Table 3. Interestingly, total olefin-to-paraffin ratio was also enhanced with Ba addition. The reduction in *TOPR* value with H_2 mole fraction for two catalysts may be attributed to increasing hydrogenation of olefinic species on catalyst surface to paraffins.

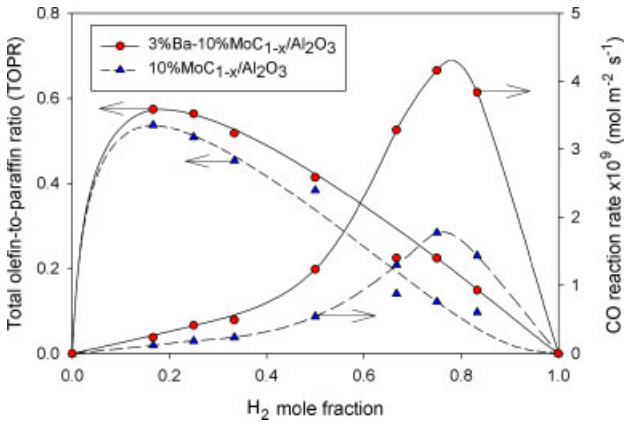

Figure 4. Effect of feed composition on Fischer–Tropsch activity of promoted and unpromoted $10\%MoC_{1-x}/Al_2O_3$ catalysts at 473 K.

As seen in Table 4, the Mo carbide catalyst system exhibited comparable FT activity to that of conventional FT catalysts even though FTS evaluation runs were conducted at atmospheric pressure in this study. Hence, MoC_{1-x}/Al_2O_3 catalysts may be potential alternative catalysts for Co- and Fe-based catalysts.

Table 4. Comparison of CO consumption rate for Mo carbide and conventional FT catalysts at H_2:CO=2:1

Catalyst	FT reaction conditions		CO consumption rate $\times 10^9$ (mol m^{-2} s^{-1})	Reference
	Temperature (K)	Pressure (atm)		
20%Co/Al_2O_3	493 K	20 atm	4.31	38
10%Co–10%Mo/Al_2O_3	493 K	20 atm	0.50	38
4%K–6%Co–1%Mo/SiO_2	523 K	1 atm	0.52	4, 39
4%K–6%Co/SiO_2	523 K	1 atm	1.59	4, 39
10%MoC_{1-x}/SiO_2	473 K	1 atm	2.65	25
10%MoC_{1-x}/ZrO_2	473 K	1 atm	1.92	25
10%MoC_{1-x}/Al_2O_3	473 K	1 atm	1.30	This work
3%Ba–10%MoC_{1-x}/Al_2O_3	473 K	1 atm	3.28	This work

Table 5. Fischer–Tropsch product selectivity over promoted and unpromoted Mo carbide catalysts at 473 K and H_2/CO=2:1

Catalyst	CO conversion (%)	Hydrocarbon selectivity (%)			
		CH_4	Olefin (C_{2+})	Paraffin (C_{2+})	C_{5+}
10%MoC_{1-x}/Al_2O_3	4.76	69.52	18.55	9.67	2.35
3%Ba–10%MoC_{1-x}/Al_2O_3	9.65	58.49	16.97	17.21	6.43

Fischer–Tropsch product selectivity

Hydrocarbon product distribution in Fischer–Tropsch synthesis generally followed a polymerization scheme and hence, hydrocarbon formation rate r_n with carbon number n may be expressed by an Anderson–Schulz–Flory (ASF) model[27] given as

$$r_n = k_{ASF}\,(1-\alpha)^2\,\alpha^{n-1} \tag{7}$$

with α and k_{ASF} being chain growth factor and Anderson-Schulz-Flory constant, respectively. As seen in Fig. 5, FT product distribution over unpromoted 10%MoC_{1-x}/Al_2O_3 catalyst exhibited good agreement with the ASF model. However, the nonlinear ASF plot was observed for promoted catalyst with two chain growth probabilities (low α_1 for C_1–C_6 and high α_2 for C_{7+}) indicating different polymerization mechanisms. The deviation in ASF product distribution suggested the possible existence of two different propagation sites (BaO.MoO_3 and MoC_{1-x} phases as seen in Fig. 1) on the catalyst surface.[40] In fact, Bian *et al*. also found that MoO_3 was the active site for hydrocarbon production.[41]

The effect of feed composition on chain growth probability of Mo carbide catalysts is depicted in Fig. 6. Both catalysts had the highest chain growth factor at a H_2 mole fraction of around 0.25–0.33. However, chain growth probability decreased with increasing y_{H_2} beyond 0.33 probably due to an increasing termination rate to propagation rate ratio. Ba promoter improved α value up to 93% (from α =0.43 to 0.83) in agreement with an increase in C_{5+} selectivity and CH_4 suppression (cf. Table 5).

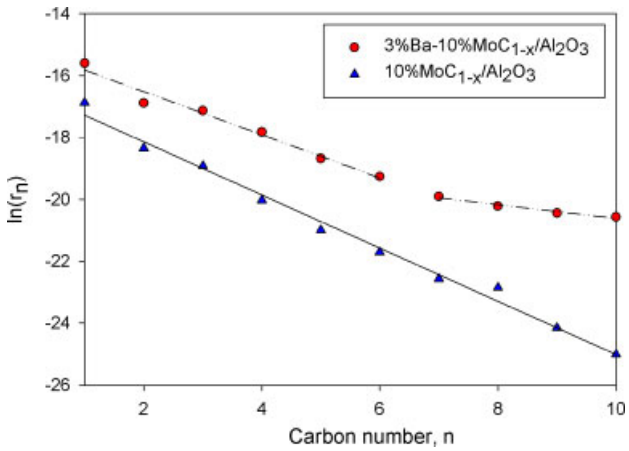

Figure 5. ASF plots for promoted and unpromoted Mo carbide catalysts at 473 K and H_2/CO=2:1.

CONCLUSIONS

XRD measurements indicated that Mo carbide particles were finely (6–10 nm) dispersed on Al_2O_3 support surface. Both α- and β-MoC_{1-x} phases were detected on promoted and unpromoted Mo carbide catalysts. The oxycarbide intermediate form produced during carburization was converted completely to the final carbide phase. Ba addition improved carbide formation rate and reduced activation energy for the formation of both carbide phases. Specific basic site strength and CO_2 uptake of the strong basic site were also enhanced with promoted catalyst while the acid properties (NH_3 uptake, heat of desorption and specific site strength) of S-acid site were reduced by Ba promotion. FT activity increased with H_2 mole fraction and reached the optimal value at $y_{H_2} = 0.75$ for both catalysts. Promoted catalyst exhibited higher CO consumption rate, total olefin-to-paraffin ratio and C_{5+} selectivity than the undoped MoC_{1-x} catalyst but reduced CH_4 selectivity. Ba promoter increased chain growth probability about 93%. The deviation of product distribution from standard ASF plots with two chain growth factors for the 3wt%Ba–10%MoC_{1-x}/Al_2O_3 catalyst was probably due to the presence of different active sites for chain initiation.

ACKNOWLEDGEMENT

The authors are grateful to the Australian Research Council (ARC) for supporting the research program in the Reactor Engineering & Technology Group, UNSW through a Discovery Grant.

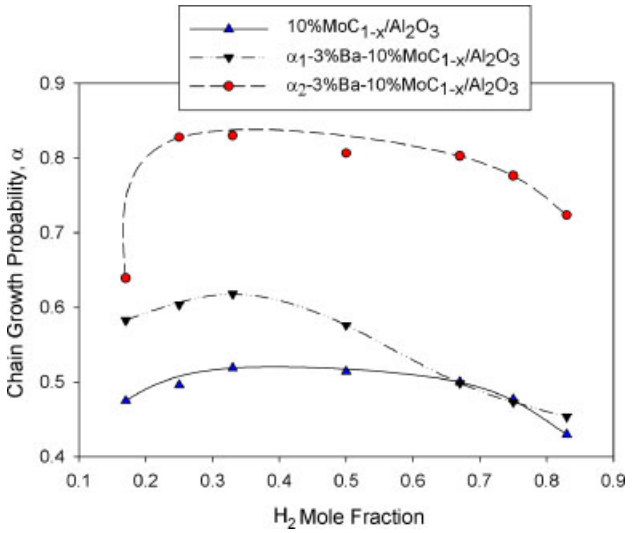

Figure 6. Effect of H_2 mole fraction on chain growth probability of promoted and unpromoted Mo carbide catalysts at 473 K.

REFERENCES

1 Tsakoumis NE, Rønning M, Borg Ø, Rytter E and Holmen A, Deactivation of cobalt based Fischer-Tropsch catalysts: a review. *Catal Today* **154**:162–182 (2010).
2 Vo DVN and Adesina AA, Fischer-Tropsch synthesis over alumina-supported molybdenum carbide catalyst. *Appl Catal A: Gen* **399**:221–232 (2011).
3 Furimsky E, Metal carbides and nitrides as potential catalysts for hydroprocessing. *Appl Catal A: Gen* **240**:1–28 (2003).
4 Chen H and Adesina AA, Improved alkene selectivity in carbon monoxide hydrogenation over silica supported cobalt-molybdenum catalyst. *Appl Catal A: Gen* **112**:87–103 (1994).
5 Levy RL and Boudart M, Platinum-like behavior of tungsten carbide in surface catalysis. *Sci* **181**:547–549 (1973).
6 Kojima R and Aika KI, Molybdenum nitride and carbide catalysts for ammonia synthesis. *Appl Catal A: Gen* **219**:141–147 (2001).
7 Yao Z and Shi C, Development of a catalytic cycle in molybdenum carbide catalyzed NO/CO reaction. *Catal Lett* **130**:239–245 (2009).
8 Claridge JB, York APE, Brungs AJ, Marquez-Alvarez C, Sloan J, Tsang SC and Green MLH, New catalysts for the conversion of methane to synthesis gas: molybdenum and tungsten carbide. *J Catal* **180**:85–100 (1998).
9 Setthapun W, Bej SK and Thompson LT, Carbide and nitride supported methanol steam reforming catalysts: parallel synthesis and high throughput screening. *Top Catal* **49**:73–80 (2008).
10 Patt J, Moon DJ, Phillips C and Thompson L, Molybdenum carbide catalysts for water-gas shift. *Catal Lett* **65**:193–195 (2000).
11 Dhandapani B, Clair TSt and Oyama ST, Simultaneous hydrodesulfurization, hydrodeoxygenation, and hydrogenation with molybdenum carbide. *Appl Catal A: Gen* **168**:219–228 (1998).
12 Li S, Lee JS, Hyeon T and Suslick KS, Catalytic hydrodenitrogenation of indole over molybdenum nitride and carbides with different structures. *Appl Catal A: Gen* **184**:1–9 (1999).
13 Zhao L, Sotoodeh F and Smith KJ, Increased surface area of unsupported Mo_2C catalyst by alkali-treatment. *Catal Commun* **11**:391–395 (2010).
14 Kim HG, Lee KH and Lee JS, Carbon monoxide hydrogenation over molybdenum carbide catalysts. *Res Chem Intermed* **26**:427–443 (2000).
15 Ranhotra GS, Bell AT and Reimer JA, Catalysis over molybdenum carbides and nitrides. II. Studies of carbon monoxide hydrogenation and ethane hydrogenolysis. *J Catal* **108**:40–49 (1987).
16 Oyama ST, Preparation and catalytic properties of transition metal carbides and nitrides. *Catal Today* **15**:179–200 (1992).
17 Hyeon T, Fang M and Suslick KS, Nanostructured molybdenum carbide: sonochemical synthesis and catalytic properties. *J Am Chem Soc* **118**:5492–5493 (1996).
18 Nelson JA and Wagner MJ, High surface area Mo_2C and WC prepared by alkalide reduction. *Chem Mater* **14**:1639–1642 (2002).
19 Preiss H, Meyer B and Olschewski C, Preparation of molybdenum and tungsten carbides from solution derived precursors. *J Mater Sci* **33**:713–722 (1998).
20 Lee JS, Locatelli S, Oyama ST and Boudart M, Molybdenum carbide catalysts 3. Turnover rates for the hydrogenolysis of n-butane. *J Catal* **125**:157–170 (1990).
21 Volpe L and Boudart M, Compounds of molybdenum and tungsten with high specific surface area. II. Carbides. *J Solid State Chem* **59**:348–356 (1985).
22 Xiao T, Wang H, Da J, Coleman KS and Green MLH, Study of the preparation and catalytic performance of molybdenum carbide catalysts prepared with C_2H_2/H_2 carburizing mixture. *J Catal* **211**:183–191 (2002).
23 Xiao T, York APE, Coleman KS, Claridge JB, Sloan J, Charnock J and Green MLH, Effect of carburising agent on the structure of molybdenum carbides. *J Mater Chem* **11**:3094–3098 (2001).
24 Nguyen TH, Nguyen TV, Lee YJ, Safinski T and Adesina AA, Structural evolution of alumina supported Mo-W carbide nanoparticles synthesized by precipitation from homogeneous solution. *Mater Res Bull* **40**:149–157 (2005).
25 Vo DVN and Adesina AA, Kinetics of the carbothermal synthesis of Mo carbide catalyst supported on various semiconductor oxides. *Fuel Process Technol* **92**:1249–1260 (2011).
26 Vo DVN, Cooper CG, Nguyen TH, Adesina AA and Bukur DB, Evaluation of alumina-supported Mo carbide produced via propane carburization for the Fischer-Tropsch synthesis. *Fuel* **93**:105–116 (2012).
27 Anderson RB, *The Fischer-Tropsch Synthesis*. Academic Press, New York (1984).
28 Vo DVN, Nguyen TH, Kennedy EM, Dlugogorski BZ and Adesina AA, Fischer-Tropsch synthesis: effect of promoter type on alumina-supported Mo carbide catalysts. *Catal Today* **175**:450–459 (2011).
29 JCPDS Powder Diffraction File, International Centre for Diffraction Data, Swarthmore, PA (2000).
30 O'Hare PAG, Thermochemistry of molybdates III. Standard enthalpy of formation of barium molybdate, and the standard entropy and standard Gibbs energy of formation of the aqueous molybdate ion. *J Chem Thermodynamics* **6**:425–434 (1974).
31 Szalier T, Kwak JH, Kim DH, Szanyi J, Wang C and Peden CHF, Effects of Ba loading and calcination temperature on $BaAl_2O_4$ formation for BaO/Al_2O_3 NO_x storage and reduction catalysts. *Catal Today* **114**:86–93 (2006).
32 Patterson AL, The Scherrer formula for X-Ray particle size determination. *Phys Rev* **56**:978 (1939).
33 York APE, Claridge JB, Williams VC, Brungs AJ, Sloan J, Hanif A, Al-Megren H and Green MLH, Synthesis of high surface area transition metal carbide catalysts. *Stud Surf Sci Catal* **130**:989–994 (2000).
34 Vo DVN and Adesina AA, A potassium-promoted Mo carbide catalyst system for hydrocarbon synthesis. *Catal Sci Technol* **2**:2066–2076 (2012).
35 Kissinger HE, Reaction kinetics in differential thermal analysis. *Anal Chem* **29**:1702–1706 (1957).
36 Solymosi F and Bugyi L, Effects of potassium on the chemisorption of CO_2 and CO on the Mo_2C/Mo(100) surface. *Catal Lett* **66**:227–230 (2000).
37 Bukur DB, Mukesh D and Patel SA, Promoter effects on precipitated iron catalysts for Fischer-Tropsch synthesis. *Ind Eng Chem Res* **29**:194–204 (1990).
38 Cooper CG, Nguyen TH, Lee YJ, Hardiman KM, Safinski Tomasz, Lucien FP and Adesina AA, Alumina-supported cobalt-molybdenum catalyst for slurry phase Fischer-Tropsch synthesis. *Catal Today* **131**:255–261 (2008).
39 Chen H, PhD thesis, The University of New South Wales, Sydney, Australia (1995).
40 Dictor RA and Bell AT, Fischer-Tropsch synthesis over reduced and unreduced iron oxide catalysts. *J Catal* **97**:121–136 (1986).
41 Bian GZ, Fan L, Fu YL and Fujimoto K, High temperature calcined K-MoO_3/γ-Al_2O_3 catalysts for mixed alcohols synthesis from syngas: effects of Mo loadings. *Appl Catal A: Gen* **170**:255–268 (1998).

